Available online at www.sciencedirect.com
ScienceDirect
International Journal of Heat and Mass Transfer 51 (2008) 1728–1737
International Journal of HEAT and MASS TRANSFER
www.elsevier.com/locate/ijhmt

Condensation heat transfer enhancement in the presence of non-condensable gas using the interfacial effect of dropwise condensation

Xue-Hu Ma *, Xing-Dong Zhou, Zhong Lan, Yi-Ming LI, Yu Zhang

Department of Chemical Engineering, Dalian University of Technology, Dalian 116012, China

Received 9 November 2006; received in revised form 9 July 2007
Available online 12 September 2007

Abstract

Heat transfer characteristics of dropwise condensation (DWC) were experimentally studied on a vertical plate for a variety of non-condensable gas (NCG) concentration, saturation pressure, and surface sub-cooling degree. As the heat transfer performance was dominated by the vapor diffusion process near the interface of the gas–liquid within the gas phase, the additional thermal resistance of the coating layer may not be strictly limited, a fluorocarbon coating was applied to promote dropwise condensation mode. Compared with the traditional filmwise condensation (FWC), heat and mass transfer with NCG can be enhanced with the dropwise condensation mode. In the present paper, the effect of condensate liquid resistance should not be regarded as the most vital factor to explain the results, but the vapor diffusion process. This is attributed to the liquid–vapor interfacial perturbation motion caused by coalescence and departure of condensate droplets. The results also demonstrated that the feature of droplets departure is the dominant factor for the steam–air condensation heat transfer enhancement.

Keywords: Non-condensable gas; Fluorocarbon coatings; Dropwise condensation; Heat transfer enhancement; Interfacial effect

1. Introduction

The presence of NCG in condensation has a great effect on heat transfer efficiency. It has been found that a very small amount of NCG can result in a significant reduction in heat transfer performance [1–5]. But such cases can be encountered frequently in many practical applications, such as the passive containment cooling system in nuclear power plant, seawater desalination system, toxic components cleaning from the exhaust gases, absorption and energy recovery system etc. Therefore, condensation of vapor in the presence of non-condensable gas is an important process in practical industry. Minkowycz and Sparrow [5] investigated the effects of the interfacial resistance, vapor superheat and other parameters on the heat transfer properties. In general, the reduction in heat transfer is due entirely to the diffusion resistance of the steam–air boundary layer. The influence of the NCG is accentuated at lower pressure levels. Moreover, the performance of the condenser is significantly degraded with NCG concentration increasing, especially for lighter gases [6]. The condensation heat transfer rate can be enhanced by increasing the inlet steam flow rate and pressure [7]. Vapor velocity can help reduce the building up of non-condensable gases at the vapor/liquid interface, hence to improve the heat transfer rate. The presence of NCG leads to different dominant resistance, the condensate film thermal resistance did not significantly affect the overall thermal resistance in the presence of NCG. Corradini [8] proposed a method to calculate the detrimental effects of the presence of non-condensable gases on absorption refrigeration system. The reduction in the heat and mass transfer as a result of

* Corresponding author. Tel.: +86 411 83653402; fax: +86 411 3633080.
E-mail address: xuehuma@dlut.edu.cn (X.-H. Ma).

0017-9310/$ - see front matter © 2007 Elsevier Ltd. All rights reserved.
doi:10.1016/j.ijheatmasstransfer.2007.07.021

Nomenclature

A	surface area, m^2
c	mole concentration, mol m^{-3}
c_p	thermal capacity, J kg^{-1} K^{-1}
d	coating layer thickness, m
D	mass diffusion coefficient, m^2 s^{-1}
g	specific force of gravity, m s^{-2}
h	heat transfer coefficient, kW m^{-2} K^{-1}
h_{fg}	latent heat of condensation, kJ kg^{-1}
k	condensate thermal conductivity, W m^{-1} K^{-1}
L	radius of condensing block, m
m	mass of the specimen, g
M	condensing drop surface area, m^2
P	condensing pressure, kPa
q	heat flux, kW m^{-2}
R	specific ideal-gas constant, J mol^{-1} K^{-1}
r	radius of condensing drop, m
S	slope of curve of logarithm temperature versus time
T	temperature, K
W_∞	air mole concentration, %

Greek symbols

$\triangle T$	temperature difference in coating layer, K
μ	viscosity, Pa s
ρ	density, kg m^{-3}
λ	thermal conductivity of coating layer, W m^{-1} K^{-1}
θ	contact angle, °

Subscripts

b	condensing block
c	coating film
l	condensate
i	thermocouple position
∞	gas phase bulk
s	saturation
v	vapor
w	condensing wall
0	bare surface
1	coated surface

non-condensable gas existence can be offset by introducing turbulence into the vapor/gas mixture in the absorber. Such effects in this process were also confirmed by Maheshwari et al. [9]. Taking regard of condensate film, they indicated that the thermal resistance of the gas boundary layer is higher than that of the condensate film for low Reynolds number, but this result may get reversed at higher Reynolds number. Semiat and Galperin [10] investigated the effects of NCG in seawater desalination on the condensation of steam outside vertical tubes. The NCG concentration distribution, temperature profiles in steam boundary layer, condensation heat transfer coefficients and the thickness of the condensate layer along the tube were obtained.

Kim and Kang [11], Karapantsios et al. [12] measured the condensation heat transfer rate for steam–air mixtures in direct contact with the sub-cooled water layers. The condensation heat transfer coefficients were found to be dependent not only on the steam concentration but also on the wave characteristics of the falling liquid layer, and the dominant factors were attributed to the dynamic interaction between the interfacial waves and the adjacent gas layer. Park et al. [13,14] dealt with the enhanced condensation heat transfer by the waviness of condensate film within the diffusion layer of a steam–air mixture in a vertical rectangular duct.

It is well known that the heat transfer characteristics of the filmwise mode can be enhanced by the wavy condensate film adjacent the gas boundary layer. For the dropwise condensation process, the interfacial effects on heat and mass transport process due to the growth-up, coalescence and departure behaviors of the condensing droplets should be introduced obviously, as shown in Fig. 1, especially in the case of high concentration of the non-condensable gas. However, there is no research considering this interfacial effect. Most of previous work [15–21] investigated the effects of condensate resistance and lower air concentration on the condensation heat transfer of a pure vapor and diminishing the effect of non-condensable gas by increasing the steam flow velocity and draining the gas near the condensing surface. Ronald et al. [17], based on kinetic theory, investigated the microscopic behavior of the diffusion-controlled dropwise condensation with a non-condensable gas, and the proposed mechanism of the vapor diffusion was used to explain the effect of NCG on heat flux. Ganzevles and co-workers [20] studied heat transfer characteristics of the condensate drops in polymer heat exchanger, it was found that mixing and convection in the condensate, caused by coalescence and drainage of drops, reduces the condensate thermal resistance as compared with purely conductive heat transfer. Jackson et al. [21] investigated

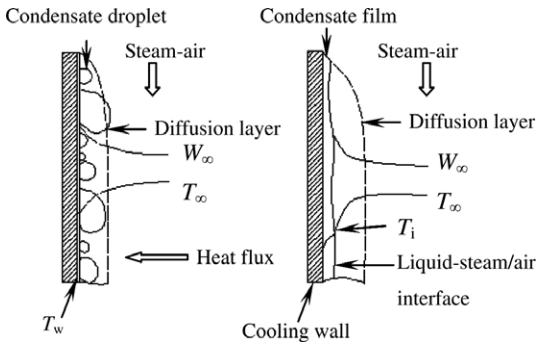

Fig. 1. Schematic diagram of DWC and FWC of steam–air mixtures.

the steam–air mixture condensation heat transfer characteristics on a flat plate. The results indicated the heat transfer rate with the plate mounted at 45° was only slightly lower than for the vertical case and the pattern of behavior with increase of air concentration was similar. The rate of heat transfer with the horizontal plate was generally lower by about 15–20% than that with the vertical one. Adequate attention has not been paid to the dropwise condensation in the presence of non-condensable gas, especially to the dynamic effect of condensing droplets on the diffusion layer of gas phase. For dropwise condensation mode of a pure vapor, higher heat transfer coefficients compared with filmwise condensation have been reported in the literature [22–25]. However, when a non-condensable gas existing in the condensing vapor, to reduce the thermal resistance of condensate layer is no more profitable due to the dominant thermal resistance resides in the gas phase. Usually various kinds of techniques are employed to enhance the mass transfer rate in the diffusion layer. The main goals of these methods can be exclusively converged to enhance the disturbance in the flow boundary layer and reduce the thickness of diffusion layer.

The objective of the present paper is to study the condensation heat and mass transfer characteristics of steam in the presence of a non-condensable gas (air) by dropwise condensation mode. From the comparison with filmwise condensation, the enhancement mechanism of the heat transfer is analyzed in terms of the interface effects of condensing droplets.

2. Heat transfer characteristics of fluor-carbon coating layer

Many methods can be applied to promote DWC mode [26–31], such as applying organic promoter, plating novel metal or metal compounds, coating low surface energy polymeric film, ion implanting et al. Unfortunately, these methods have not been effectively applied in industrial condensers so far because the specific low energy surface materials for sustaining long-term DWC have not yet been successfully manufactured. As an alternative, polymer coating seems to be a very promising method in industrial applications [26,27]. One of these materials is fluorocarbon polymer for the desirable characteristics of high thermal stability and low surface energy. The higher resistance to chemical attack is another merit of fluorocarbon polymers when applying in the vapor mixtures with corrosive components. But, there are still two contradictory problems, i.e. the adhesion to the substrate and the thickness relating to the additional thermal resistance of the polymer layer, have to be settled in prior. Applying fluorocarbon organic compounds should be modified firstly to obtain a well conductive and low surface energy coating layer. The maximum thickness of coating layer should be less than 5 μm in dropwise condensation for pure vapor; otherwise the additional thermal resistance can offset the enhanced efficiency from altering the mode [28]. For the condensation of steam–air mixture vapor, the two crucial problems mentioned above are no more difficult to be resolved. As the dominated thermal resistance resides within the steam–air boundary layer, an appropriate thickness of the coating surface promoting dropwise condensation mode and sustaining enough durability for realizing long-term dropwise condensation is viable especially in the case of high concentration of non-condensable gas. The additional thermal resistance of the organic may not be strictly limited and the thickness of the coating film can be relatively high. The modified coating layer used in this paper was composed of two interacted layers, the compact bottom layer and the low surface energy upper layer. The bottom layer was well adhered to the solid substrate by introducing nano-metal particles, and thus was regarded as a transition region connected to the low energy upper layer. The compact and stable fluorocarbon coating layer was prepared with static contact angle 85.2°. The contact angle was measured by the measurement apparatus Dataphysics OCAH200.

The thermal conductivity of the coating layer material used in condensation process was measured experimentally by the transient comparative exponential method (CEM). The main theoretical basis of the CEM was described in detail in reference [32]. In the present paper, copper and aluminum were used as the substrate specimen. The samples ($20 \times 20 \times 1$ mm) were simultaneously immersed in boiling water (100 °C) for the transient temperature measurement at the backside of the substrate by Agilent34970A data acquisition system with a high speed card. The measurements were conducted for eight times for each specimen. By making a plot of the logarithm temperature versus time, the slope of the linear curve was gained, shown in Fig. 2. The thermal conductivity of the coating layer can be calculated using Eq. (1).

$$\lambda_c = \frac{C_p \cdot d \cdot m}{A(1/S_1 - 1/S_0)} \tag{1}$$

where S_0 and S_1 represent the average slopes of the linear curves for pure substrate and coated substrate, respectively.

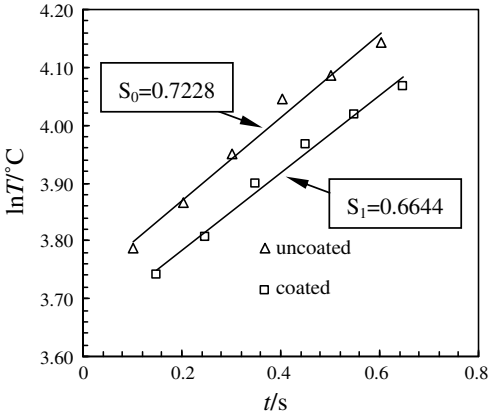

Fig. 2. Logarithm temperature ($\ln T$) versus elapsed time (t) for the sample in condition of 100 °C.

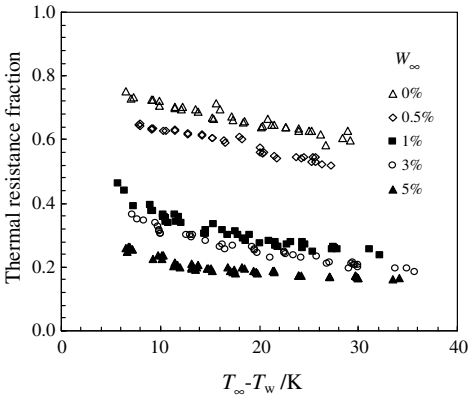

Fig. 3. Thermal resistance fraction of the coating layer in the condensing process in the presence of non-condensable gas.

The coating layer thickness d is measured by SEM ($d = 14.6 \pm 0.1$ μm). The average conductivity of the coating layer ($\lambda = 0.61 \pm 0.05$ W m^{-1} K), was achieved from eight times measurement for the specimens.

For the coating film used in condensation heat transfer experiments, the thickness of coating layer was measured by a non-destroy method, BYKO-test 7500 coating thickness measurement gauge, with the uncertainty of $\pm 2\% + 1$ μm.

As a preliminary experiment, the thermal resistance over the coating layer was tested at conditions of 0.5% and 5% air molar concentration. The thermal resistance ratio of the thermal driving force in the promoting layer ($\Delta T = q \cdot d/\lambda_c$) to the overall temperature difference between vapor and copper surface ($T_\infty - T_w$), is shown in Fig. 3. The resistance ratio decreases as the concentration of air and the surface sub-cooling degree increases. For the air concentration of 0.5%, the resistance ratio is about 50–65%, but it is only 15–25% when concentration of air up to 5%. These results confirm that it is feasible to utilize the modified coating layer in condensation heat transfer of vapor in presence of NCGs.

3. Experiments

The condensation experiment schematic diagram is shown in Fig. 4. This experiment loop is composed of four main sub-loops, the air–vapor mixture, cooling water, condensate removal, and data acquisition and control system. The filtered air, as non-condensable gas came from an oil-free air compressor, passed through a pressure regulator, flow meter, and then entered into the bottom of the electrically heated boiler. The steam–air mixture vapor was generated in the boiler and the temperature was controlled by silicon controllable rectifier. The steam–air mixture passed through a vapor–liquid separator, flow rate control valve before flowing into the condensing chamber. Moreover, at the entrance of the condensing chamber, a buffer device was installed in order to eliminate the heat and mass transfer influence resulting from the entrance effect of vapor flowing. Steam–air loop can be regulated at a constant pressure based on the experiment condition. Flow velocity of the steam–air mixture at the condensing chamber is less than 0.8 m s^{-1}, which can be obtained indirectly by calculation from the entering air flow rate, air concentration and the cross-section area of the condensing chamber in the flow direction. The condensation chamber is made of stainless steel. Pressure were measured with a manometer with an uncertainty of ±0.1% of the full scale (0–100 kPa), and the ambient pressure was determined with a standard mercury barometer. Four windows were mounted at the chamber so that condensing observation and photography can be taken. The excess mixtures from test section go via an auxiliary condenser discharged to atmosphere by a vent valve.

A cylindrical condensing surface, 30 mm in diameter and 4l0 mm long, is made of high purity copper. The

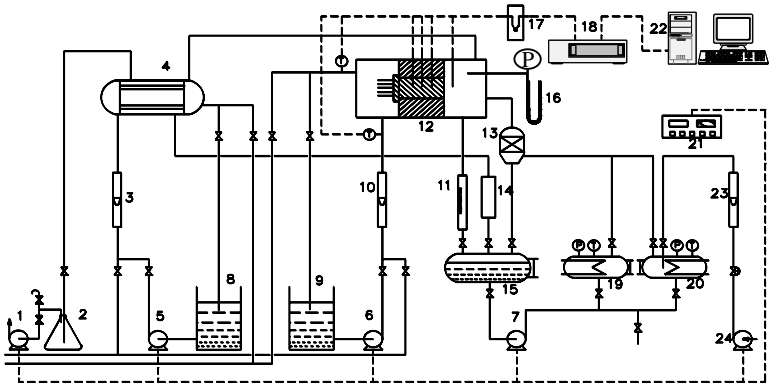

Fig. 4. Schematic of experimental set-up. (1) vacuum pump; (2) vapor–liquid separator; (3, 10, 23) flow meters; (4) auxiliary condenser; (5, 6, 7, 24) water pump; (16) U type pressure manometer and transducer; (17) thermocouple cold point; (18, 22) data acquisition system; (19, 20) boiler; (21) power controller; (8, 9) cooling water tank; (11) condensate measuring tube; (2) condenser; (13) vapor/water separator; (14) buffer vessel; (15) stock tank.

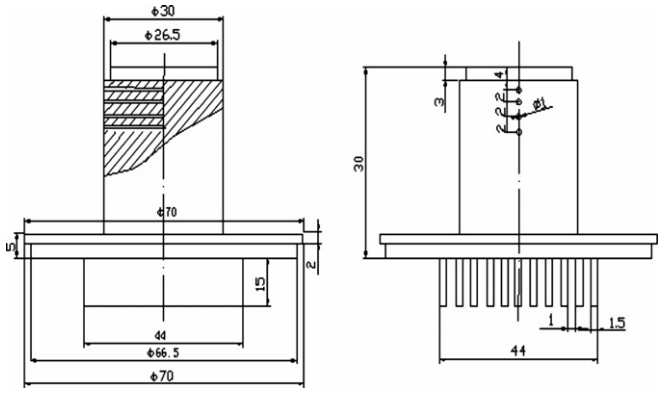

Fig. 5. Experimental condensing block (dimension unit: $\times 10^{-3}$ m).

condensing surface is oriented vertically. Four holes with 0.8 mm diameter are drilled into the block parallel with each other, perpendicular to the axis, with copper-constantan thermocouple inserted into it. The thermocouple arrangement is shown in detail in Fig. 5. All copper-constantan thermocouples used in the experiments are calibrated in a high-precision constant-temperature bath against a standard platinum resistance thermometer calibrated by the National Metrical Laboratory of China. A polynomial is fitted to the combined data for every thermocouple, compare to the standards platinum resistance thermometer the deviation of the calibrated T type thermocouple is within ±0.05 °C.

The condensing block is thermally insulated with PTFE to assure the one-dimensional conduction within the condensing block. Experimental data are collected with Agilent34970A data acquisition system, and all of the data including pressure, thermocouple readings, surface sub-cooling temperature, non-condensable gas concentration, heat flux, condensation heat transfer coefficients can be calculated by data reduction software, and the real-time data profiles can be displayed on the computer monitor. The linearity among the four readings of thermocouples embedded in the condensing block is checked by the instantaneously reduced data displayed on computer monitor. When the linearity is greater than 0.98, the experimental results are considered to be effective.

Heat transfer surface at cooling side is extended with 15 rectangular fins, as shown in Fig. 5, to match the dropwise condensation heat transfer capacity. Water as the coolant is supplied by constant-temperature bath. All the experiments are repeated under the same operation conditions the other day.

4. Experimental data reduction

The heat flux is determined using the least squares method from the thermocouple readings in the condensing block. The surface temperature is calculated by extrapolating the temperature gradient to the condensation surface. At each time interval, the instantaneous heat flux and surface temperature are calculated from Eqs. (1) and (2), respectively:

$$q = -\lambda_b \frac{\sum_{i=1}^{4}(x_i - \bar{x})(t_i - \overline{T})}{\sum_{i=1}^{4}(x_i - \bar{x})^2} \tag{2}$$

$$T_W = \overline{T} + \frac{q}{\lambda_b}\bar{x} \tag{3}$$

$$\bar{x} = \frac{1}{4}\sum_{i=1}^{4} x_i, \quad \overline{T} = \frac{1}{4}\sum_{i=1}^{4} T_i \tag{4}$$

The average heat flux q and surface temperature T_w at all the time range are then calculated under steady-state conditions. The dropwise condensation heat transfer coefficient is calculated from:

$$h = \frac{q}{(T_\infty - T_w)} \tag{5}$$

It should be noted that the surface sub-cooling temperature includes the temperature difference across the coating layer, condensate layer and the gas–steam mixtures buffer layer.

Filmwise condensation of pure steam at atmospheric pressure is also performed as the first step for comparison with the modified Nusselt theory calculation values to check the validity of experiment system. The modified condensation heat transfer coefficient for a vertically-oriented cylindrical plate is derived by O'Neill and Westwater [33] as follows,

$$h = 0.83404\left[\frac{k_l^3 \rho_l^2 g h_{fg}}{\mu_l L(T_s - T_w)}\right]^{\frac{1}{4}} \tag{6}$$

Thermocouples and pressure transducers are installed at about 15 mm from the condensing surface to monitor the condensing temperature, and calculate the concentration of NCG. The mole concentration of NCG in steam–air mixture is calculated from Gibbs–Dalton ideal gas mixture equation, as shown in Eq. (7).

$$W_\infty = \frac{P_\infty - P_s(T_\infty)}{P_\infty} \tag{7}$$

The uncertainties of the measured and calculated parameters are estimated by the procedure described by Kline and McClintock [34,35]. The experimental uncertainties associated with the sensors and calculated parameters are listed in Table 1.

Table 1
Experimental uncertainties

Sensors	
Temperature	±0.05 °C
Pressure transducer	±0.05 kPa
Parameters	
Thermal driving force $T_\infty - T_w$	±2.4%
Condensation heat transfer coefficient	±5.7%
Condensation heat transfer flux	±2.1%
Non-condensable concentration	±0.2%

5. Experimental results and discussion

5.1. Condensate liquid characteristics

Experiments were conducted, including the system validity checking; feasibility analysis of the coating layer application in steam mixtures condensation; heat transfer characteristics comparison of FWC and DWC with air molar concentrations of 0.5%, 1%, 2%, 3% and 5%, at pressures 0.1 MPa and 0.16 MPa, respectively.

FWC was performed firstly on the copper surface before applying coating film without NCG to validate the system, as seen from Fig. 6. It is well agreed with the modified Nusselt theory data, the deviation is within ±5%. In general, the difference of the condensate feature leads to the different heat transfer characteristics. FWC is the practical condensation mode, which can be enhanced by DWC because of the condensate resistance reduction. However, when the condensation process contains some NCG, the thermal resistance of the condensate is no more important. In spite of thermal resistance of the condensate, the interfacial heat and mass transfer process would be dominated. For filmwise condensation, condensate film maintained at a quiescent state, as shown in Fig. 7a. Here, no wave at the condensate film was found in the presence of NCG. However, in the case of dropwise condensation, a quite different feature of condensate was illustrated. Droplets movement on the condensing surface was analyzed using video recording and photography. The apparent appearance can be illustrated from photographs in Fig. 7, a renewal motion of the condensing surface were recorded. The elapsed time of one cycle at the condition of 0.5% air molar concentration and 0.1 MPa of pressure was about 0.53 s. However, with the same temperature difference, for the cases of air molar concentration of 1% and 5%, the elapsed time was 2.15 s and 6.37 s, respectively. It can be found that the average renewal frequency of the condensing surface decreased with the air concentration increasing. The condensation photos in Fig. 8 also illustrated that diameter of the departing droplet was larger than the calculated critical size [36]. In general, the difference between the factual experimental data and the theory data is due to the coalescing with the larger droplets adjacent the departure droplet and the mass grow rate of the larger droplet is nonlinear. Sweeping motion of droplets yield strips of bare surface on their down way, such repeated performance created the dynamic renewal of the condensation surface.

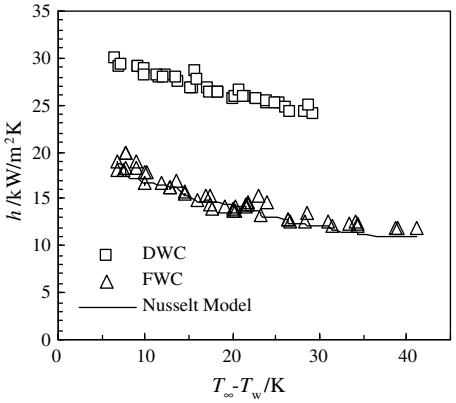

Fig. 6. Heat transfer coefficient of FWC, DWC and modified Nusselt theory calculation versus thermal driving force, at 0.1 MPa.

The experimental phenomena of DWC in the presence of NCG at condition of 0.1 Mpa, and 0.16 MPa were shown as in Fig. 7c and d. No distinct difference was found from the appearance. Only the statistic results of the renewal time of condensing surface indicated that droplet recycle time was reduced at 0.16 MPa.

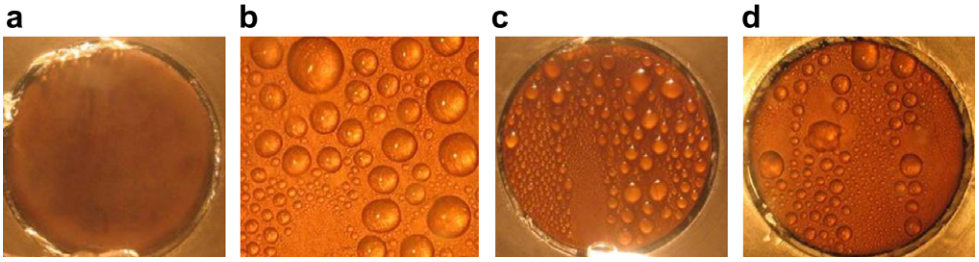

Fig. 7. Experimental phenomena ((a) FWC, (b) DWC without non-condensable gas; (c, d) DWC with non-condensable gas at 0.1 MPa and 0.16 MPa, respectively).

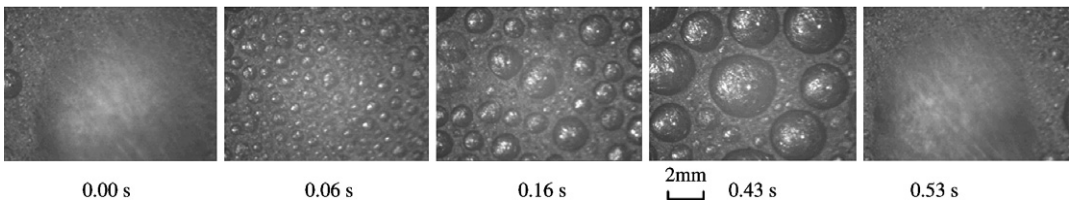

Fig. 8. Serial photographs of dropwise condensation in one renewal cycle of the condensing surface ($W_\infty = 0.5\%$, $T_\infty - T_w = 15$ K, 0.1 MPa).

5.2. Heat transfer characteristics comparison of DWC and FWC

From Fig. 9a and b, it is indicates that the condensation heat flux was reduced with increasing the air content, 1% of the air molar concentration existing in the system makes about 50% heat flux reduction. The condensation heat transfer curves have the same tend at 0.1 MPa and 0.16 MPa. Fig. 10 showed the results for the comparison of FWC and DWC heat transfer coefficients at the identical thermal driving force at 0.1 Mpa and 0.16 MPa, respectively. Condensation heat transfer coefficient can be

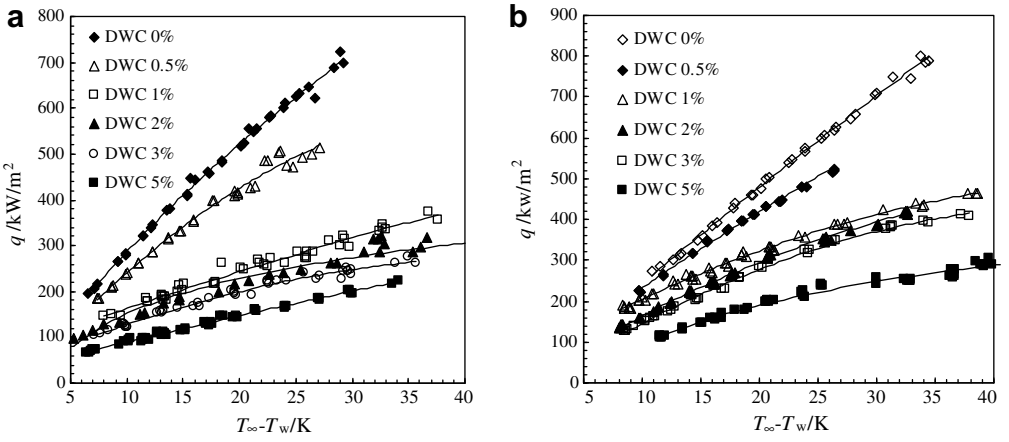

Fig. 9. Condensation heat flux versus thermal driving force, with and without non-condensable gas, at 0.1 MPa (a), 0.16 MPa (b) respectively.

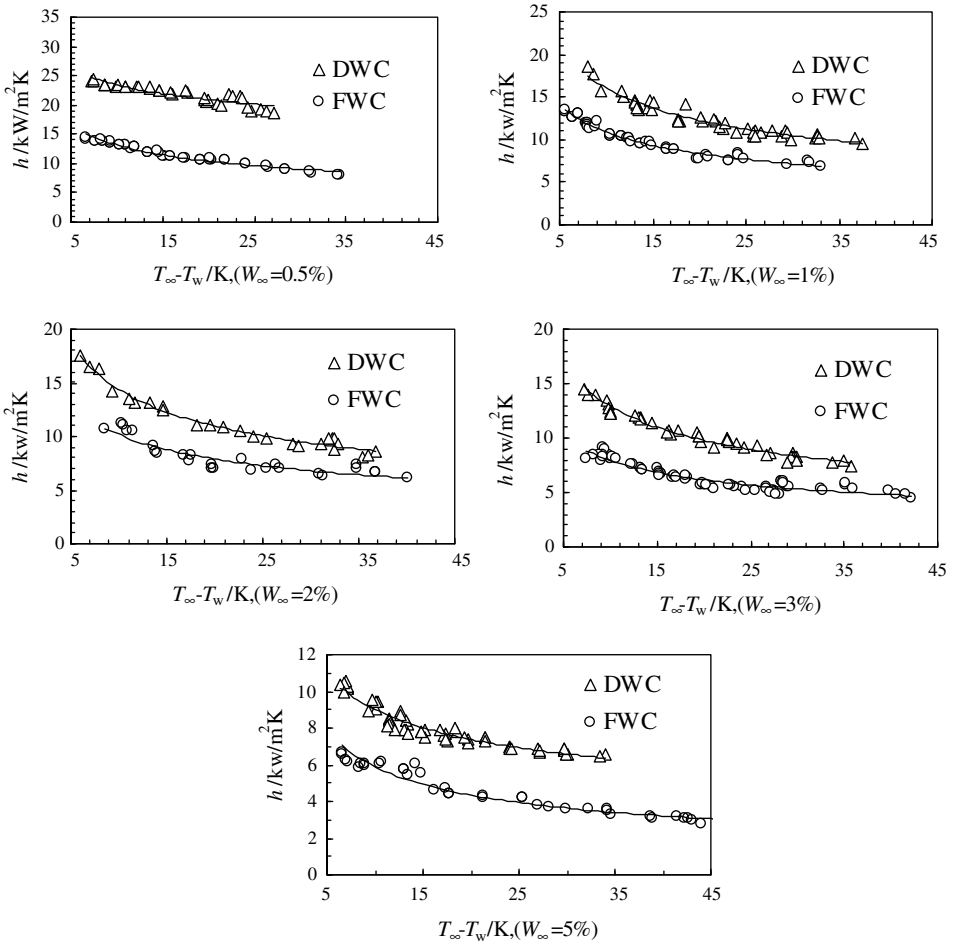

Fig. 10a. Condensation heat transfer coefficient versus thermal driving force with different non-condensable gas at 0.1 MPa.

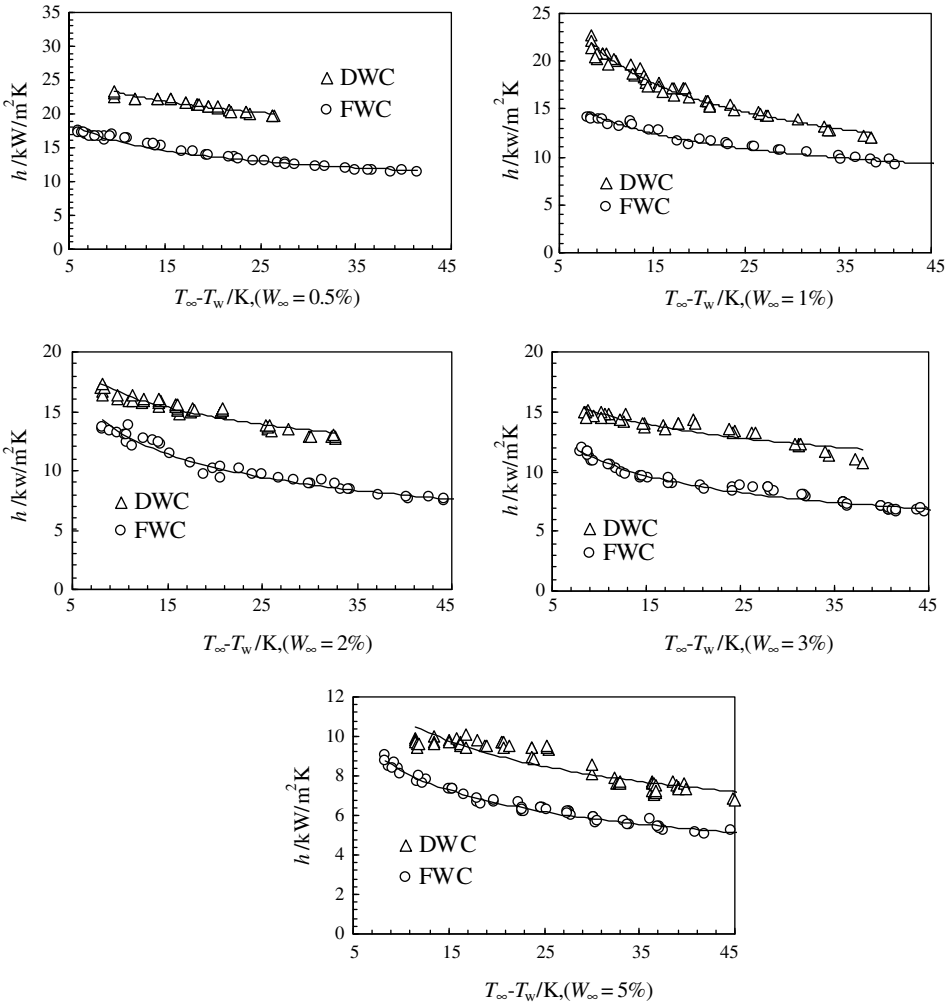

Fig. 10b. Condensation heat transfer coefficient versus thermal driving force with different non-condensable gas at 0.16 MPa.

enhanced by 30–80% in DWC mode. These results can be attributed to such factors, the area enlarge of the condensing surface, the thermal resistance reduction of the condensate and the disturbance of gas side for the special condensate drainage movement.

It is the fact that heat transfer coefficient in DWC can be several 10 times of that in FWC due to the lower thermal resistance of the condensate. However, the thickness of the condensate layer is much less than that of the vapor–gas boundary layer [5], so the thermal resistance no longer played an important role in heat transfer enhancement in the presence of NCG. Attention is paid to the effect of condensing surface, for FWC in present study, vapor molecular condensation process occurred on the condensate film. No wavy movement phenomena can be found in the whole condensing process, and the factual condensing surface area is regarded to be equivalent to the condensate film area. Whereas in DWC, it is noted that the irregular condensing surface is an important feature different from FWC. The condensing surface is covered by lots of droplets, with the increase of NCG concentration, the condensing surface area over the droplet should be taken into consideration. If the whole surface were covered by droplets, and the surface of the droplets in the shape of parts of a sphere should be considered as the condensing surface, the factual area ratio of DWC to FWC is expressed as a function of droplet contact angle, as follows, $\varphi = \frac{2\pi r^2(1-\cos\theta)}{\pi r^2 \sin^2\theta} = \frac{2}{1+\cos\theta}$. It is obvious that the condensing surface is some extent enlarged due to the increase of the droplets surface. But larger diameter droplets on the condensing surface may result in some insulating parts, hence to reduce the effective area of condensing surface. In general, vapor molecular condensing takes place on the solid surface of the trajectory of the moving droplet and the surface of some smaller droplets in DWC, while completely on the surface of the condensate film in FWC. The condensation coefficient is another factor due to the special interface of vapor–liquid during dropwise condensation process. Of the two condensing processes on the solid surface and the condensate surface, in fact, is a dynamic balance process of evaporation and condensation. There is nearly unit of the condensation coefficient when condensation occurs on the solid surface; the condensation coefficient on the solid surface is higher than that on the condensate surface owing

to the simultaneous reversal evaporation process. So that directly condensing process on solid surface resulting from the trajectory of the moving droplets in DWC is more efficient than that on liquid condensate surface in FWC [17].

The effect factors as described above may be only partial of the whole condensing process. By considering the diffusion process in the gas phase, seen from Fig. 1, both in filmwise and dropwise condensation, when the steam–air mixture vapor moves towards the cooling surface, the NCG molecules cannot penetrate through condensate layer, and thus accumulate near the interface of the condensate layer. Accordingly, the vapor temperature, the concentration and the partial pressure gradients are formed within the gas phase boundary layer. The build-up of NCG at the interface causes the reduction of vapor molecular transport to the cooling surface. In the case of the NCG molar concentration is less than 0.85, the latent heat makes the key contribution to overall heat flux and the sensible heat is negligible [12], thus the heat transfer efficiency is greatly affected by the vapor mass transfer rate from bulk vapor to the condensing surface. In the present paper, an air boundary layer is supposed to reside at the interface of gas–liquid. In FWC, the temperature and concentration fields within the boundary layer are assumed at a steady-state, and no turbulence in the diffusion layer. Consequently, the effect of the condensate film flow feature on the mass diffusion in gas phase is generally ignored, especially at low condensate flow rate. However, for dropwise condensation process, the pattern of mass diffusion boundary layer near the interface is quite different from that in FWC due to the growth and coalescence of droplets. Attention should be paid to the droplets moving behavior that leads to the peculiar condensate and steam–air interface. The growth, coalescent and departure of droplets can give rise to the irregular and variable interface, longitudinal mixing effect, transversal suction motion, and fast surface renewal rate. This sweeping motion of larger droplets gives a longitudinal mixing effect and transversal suction motion to the mass diffusion boundary layer, resulting in the enhancement of the mass diffusion process. The falling-down behavior of droplets remarkably intensifies the dense non-condensable gas/air flowing towards the condensing surface. The pulsation interface of the falling droplet may be another main factor to enhance the condensation heat and mass transfer process.

By comparison of DWC and FWC at 0.1 MPa and 0.16 MPa, it also can be found that the heat transfer characteristics of both condensate modes are enhanced with the increase of the operation pressure. For binary gas mixtures at low pressure, the mass diffusion coefficient is inversely proportional to the pressure, increases with increasing temperature, and is almost independent of the composition for the given gas pair. The relationship can be shown as $D_{AB} \propto (T)^{3/2}/P$, since the higher operation pressure corresponding to a higher steam–air temperature, accordingly, for ideal gas ($P = cRT$), it is not surprising to find that D_{AB} can be raised for a higher pressure. So the heat and mass transfer augmentation in 0.16 MPa is displayed in the experimental results because of the improvement of the molecular dynamic energy and the mass diffusion coefficient. To make a general consideration of the effect of NCG, condensation heat transfer coefficient versus non-condensable gas content with cooling water flow rate of 0.5 m^3/h at 0.1 MPa was experimentally studied. Seen from Fig. 11, the condensation heat transfer coefficient tends to decrease with the increase of the NCG concentration in DWC and FWC. The intensity of droplets movement and the extent of the heat transfer enhancement are gradually reduced with the increase of the NCG concentration.

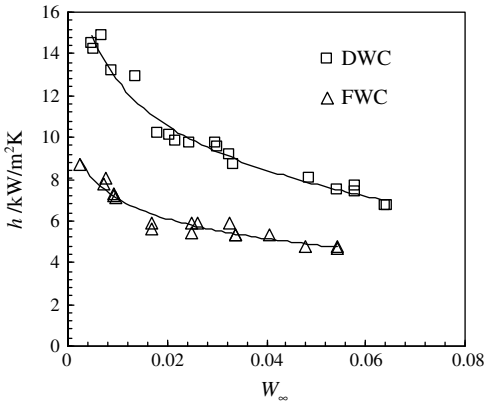

Fig. 11. Heat transfer coefficient h versus non-condensable gas content with cooling water flow rate 0.5 m^3/h, at 0.1 MPa.

6. Conclusions

Experimental investigation on heat transfer characteristics of DWC and FWC in the presence of NCG has been performed. From the experiment observation and heat transfer data comparison, the following conclusions can be drawn:

1. Fluorocarbon organic coating applied to promote DWC mode shows well physic-chemistry characteristics as the condensing surface; thermal resistance of the coating layer is no more the restriction factor in the case of condensation of steam with higher concentration of non-condensable gas.
2. The condensation heat transfer characteristics can be affected by sub-cooling degree, operation pressure and other factors for steam condensation in the presence of air. The dominated factor is the air concentration, although the existing air component seriously deteriorates the heat transfer coefficient in both DWC and FWC modes, there is still a different heat transfer nature between these two condensation modes.
3. Compared to FWC, the interfacial dynamic interaction caused by growth, coalescence and departure of droplets is a viable method for condensation heat transfer enhancement of steam–air mixture vapor. The irregular

and variable interface, longitudinal mixing effect, transversal suction motion and fast surface renewal rate may greatly improve the transport characteristics of mass diffusion layer.

4. Dropwise condensation heat transfer coefficients of steam with air concentration of 0.5–5% can be increased by 30–80% compared with those for filmwise condensation.

Acknowledgements

This work was financially supported by National Natural Science Foundation of PR China (Nos. 50376005 and 50476072).

References

[1] A.P. Colburn, O.A. Hougen, Design of cooler condensers for mixtures of vapors with noncondensing gases, Ind. Eng. Chem. 26 (1934) 1178–1182.
[2] D.W. Tanner, D. Pope, C.J. Potter, D. West, Heat transfer in DWC at low steam pressure in the absence and presence of non-condensable gas, Int. J. Heat Mass Transf. 11 (2) (1968) 181–190.
[3] D.W. Tanner, D. Pope, C.J. Potter, D. West, Heat transfer in DWC Part I. The effect of heat flux steam velocity and non-condensable gas concentration, Int. J. Heat Mass Transf. 8 (1965) 419–426.
[4] C.Y. Wang, C.J. Tu, Effects of non-condensable gas on laminar film condensation in a vertical tube, Int. J. Heat Mass Transf. 31 (11) (1988) 2339–2345.
[5] W.J. Minkowycz, E.M. Sparrow, Condensation heat transfer in the presence of non-condensables, interfacial resistance, super heating variable properties and diffusion, Int. J. Heat Mass Transf. 9 (1966) 1125–1144.
[6] V. Srzic, H.M. Soliman, S.J. Ormiston, Analysis of laminar mixed convection condensation on isothermal plates using the full boundary layer equations mixtures of a vapor and a lighter gas, Int. J. Heat Mass Transf. 42 (1999) 685–695.
[7] J.W. Rose, Approximate equation for forced convection in the presence of non-condensable gas on flat plate and horizontal tube, Int. J. Heat Mass Transf. 23 (1980) 539–546.
[8] M.L. Corradini, Turbulent condensation on a cold wall in the presence of a noncondensable gas, Nucl. Technol. 64 (2) (1984) 186–195.
[9] N.K. Maheshwari, D. Saha, R.K. Sinha, M. Ritomi, Investigation on condensation in presence of a noncondensable gas for a wide range of Reynolds number, Nucl. Eng. Des. 227 (2) (2004) 219–238.
[10] R. Semiat, Y. Galperin, Effect of non-condensable gases on heat transfer in the tower MED seawater desalination plant, Desalination 140 (2001) 27–46.
[11] M.H. Kim, H.C. Kang, Condensation phenomena with wavy interface in the presence of a noncondensable gas, Condensat. Condens. Des. ASME (1993) 219–230.
[12] T.D. Karapantsios, M. Kostoglou, A.J. Karabelas, Local condensation rates of steam–air mixtures in direct contact with a falling liquid film, Int. J. Heat Mass Transf. 38 (5) (1995) 779–794.
[13] S.K. Park, M.H. Kim, K.J. Yoo, Condensation of pure steam and steam–air mixture with surface waves of condensate film on a vertical wall, Int. J. Multiphase Flow 22 (1996) 893–908.
[14] S.K. Park, M.H. Kim, K.J. Yoo, Effects of a wavy interface on steam–air condensation on a vertical surface, Int. J. Multiphase Flow 23 (6) (1997) 1031–1042.
[15] E. Citakoglu, J.W. Rose, Dropwise condensation-some factors influencing the validity of heat-transfer measurements, Int. J. Heat Mass Transf. 11 (3) (1968) 523–537.
[16] T.G. Sundararaman, T. Venkatram, Heat transfer during DWC of steam in the presence of non-condensable gases effects of geometrical shape of the surface reversal of cooling of water flow and orientation, Ind. J. Technol. 14 (7) (1976) 313–321.
[17] R.L. Reisbig, Diffusion-controlled condensation two a two-species mixture, High Temp. High Press. 24 (2) (1992) 231–240.
[18] M. Abdulhadi, Estimation of air traces in steam–air mixtures subjected to dropwise condensation, Int. Commun. Heat Mass Transf. 14 (3) (1987) 347–351.
[19] R. Shade, B. Mikic, The Effect of non-condensible Gases on heat transfer during DWC, in: AIChE 67th Annual Meet, 1974, p. 676–681.
[20] F.L.A. Ganzevles, C.W.M. van der Geld, Temperatures and the condensate heat resistance in DWC of multicomponent mixtures with inert gases, Int. J. Heat Mass Transf. 45 (15) (2002) 3233–3243.
[21] J.D. Jackson, P. An, M. Ahmadinejad, Heat transfer from a steam/air mixture to a water cooled condensing plate, in: Proceedings of the 12th International Heat Transfer Conference, vol. 3, 2002, p. 911–916.
[22] E. Schmidt, W. Schurig, W. Sellschopp, Versuche über die Kondensation in Film-und tropfenform, Tech. Mech. Thermodynamik. I (1930) 53–63.
[23] J.W. Rose, DWC theory and experiment: a review, Proc. Inst. Eng. Part A: J. Power Energ. 216 (2001) 115–128.
[24] X.H. Ma, J.W. Rose, D.Q. Xu, J.F. Lin, B.X. Wang, Advances in DWC heat transfer: chinese research, Chem. Eng. J. 78 (2000) 87–93.
[25] X.H. Ma, J.B. Chen, D.Q. Xu, J.F. Lin, C.S. Ren, Z.H. Long, Influence of processing conditions of polymer film on DWC heat transfer, Int. J. Heat Mass Transf. 45 (16) (2002) 3405–3411.
[26] P.J. Marto, D.J. Looney, J.W. Rose, A.S. Wanniarachchi, Evaluation of organic coatings for the promotion of DWC of steam, Int. J. Heat Mass Transf. 29 (8) (1986) 1109–1117.
[27] T. Haraguchi, R. Shimada, S. Kumagai, T. Takeyama, The effect of polyvinylidene chloride coating thickness on promotion of dropwise steam condensation, Int. J. Heat. Mass Transf. 34 (12) (1991) 3047–3054.
[28] I. Tanasawa, Advances in condensation heat transfer, Adv. Heat Transf. 21 (1991) 39–55.
[29] Q. Zhao, D.C. Zhang, J.F. Lin, Surface materials with dropwise condensation made by ion implantation technology, Int. J. Heat Mass Transf. 34 (11) (1991) 2833–2835.
[30] G. Koch, K. Kraft, A. Leipertz, Study on plasma enhanced CVD coated material to promote dropwise condensation of steam, Int. J. Heat Mass Transf. 41 (13) (1998) 1899–1906.
[31] X.H. Ma, B.X. Wang, D.Q. Xu, J.F. Lin, Dropwise condensation heat transfer of steam on polymer coatings, in: International Symposium on Heat Transfer, vol. 7–11, October, 1996, p. 435–438.
[32] S. Seifert, E. Litovsky, J.I. Kleiman, R.B. Heimann, Thermal resistance and apparent thermal conductivity of thin plasma-sprayed mullite coatings, Surf. Coat. Technol. 200 (2006) 3404–3410.
[33] G.A. O'Neill, J.W. Westwater, Dropwise condensation of steam on electroplated silver surfaces, Int. J. Heat Mass Transf. 27 (9) (1984) 1539–1549.
[34] S.J. Kline, F.A. McClintock, Describing uncertainties in single-sample experiments, Mech. Eng. 75 (1953) 3–8.
[35] S.J. Wilcox, W.M. Rohsenow, Film condensation of potassium using copper condensing block for precise wall-temperature measurement, J. Heat Transf. (1970) 359–371.
[36] J.C. Min, X.F. Peng, X.D. Wang, Departure diameter of a drop on a vertical plate, J. Basic Sci. Eng. 10 (1) (2002) 51–62.